Chapter 2
Theoretical Background

This chapter gives an overview of the theory used within this project. A derivation of the non-linear wave equation is presented along with a discussion of how this is utilised. Examples of how this theory extends to practical cases such as terahertz generation in ZnTe and MgO:SLN are also given. The theory of how other terahertz generation techniques used such as the generation of terahertz radiation via the photoexcitation of large area photoconductive antennas (PCAs) is also presented. The fundamental concepts regarding charged particle acceleration are given including the requirements of the electromagnetic radiation providing the acceleration and the equations that govern the interaction. Devices used within this project such as various electronic terahertz detectors and are also described.

2.1 Non-linear Wave Equation

Maxwell's equations explain how electromagnetic radiation changes as a function of time and space and are given by [1],

$$\nabla \overline{D}(\overline{x}, t) = 4\pi\rho, \tag{2.1}$$

$$\nabla \overline{B}(\overline{x}, t) = 0, \tag{2.2}$$

$$\nabla \times \overline{E}(\overline{x}, t) = -\frac{1}{c}\frac{\partial}{\partial t}\overline{B}(\overline{x}, t), \tag{2.3}$$

$$\nabla \times \overline{H}(\overline{x}, t) = \frac{1}{c}\frac{\partial}{\partial t}\overline{D}(\overline{x}, t) + \frac{4\pi}{c}\overline{J}(\overline{x}, t), \tag{2.4}$$

M.J. Cliffe, *Longitudinally Polarised Terahertz Radiation for Relativistic Particle Acceleration*, Springer Theses, DOI 10.1007/978-3-319-48643-7_2

where $\overline{D}(\bar{x},t)$ is the electric displacement vector, ρ is the density of free charge, $\overline{B}(\bar{x},t)$ is the magnetic field vector, $\overline{E}(\bar{x},t)$ is the electric field vector, c is the speed of light in a vacuum, t is time and $\overline{J}(\bar{x},t)$ is the current density. In free space there are no free charges and therefore $\rho = 0$ and $\overline{J} = 0$. The electric displacement vector, $\overline{D}(\bar{x},t)$, can be expressed in terms of $\overline{E}(\bar{x},t)$ by

$$\overline{D}(\bar{x},t) = \overline{E}(\bar{x},t) + 4\pi\overline{P}(\bar{x},t), \tag{2.5}$$

where $\overline{P}(\bar{x},t)$ is the polarisation vector and can be thought of as a localised value of $\overline{E}(\bar{x},t)$.

From these equations and assumptions, it is possible to derive the optical non-linear wave equation. First the curl of Eq. (2.3) is taken giving,

$$\nabla \times \nabla \times \overline{E}(\bar{x},t) = -\nabla \times \frac{1}{c}\frac{\partial}{\partial t}\overline{B}(\bar{x},t). \tag{2.6}$$

Interchanging the order of the spatial and temporal derivatives on the right hand side enables $\nabla \times \overline{B}$ to be replaced with $\frac{1}{c}\frac{\partial}{\partial t}\overline{D}(\bar{x},t) + \frac{4\pi}{c}\overline{J}(\bar{x},t)$ and also remembering that $\overline{J}(\bar{x},t) = 0$ gives the following expression,

$$\nabla \times \nabla \times \overline{E}(\bar{x},t) = -\frac{1}{c^2}\frac{\partial^2}{\partial t^2}\overline{D}(\bar{x},t). \tag{2.7}$$

It is now possible to replace $\overline{D}(\bar{x},t)$ with $\overline{E}(\bar{x},t)$ by using Eq. (2.5). This gives

$$\nabla \times \nabla \times \overline{E}(\bar{x},t) = -\frac{1}{c^2}\frac{\partial^2}{\partial t^2}\left[\overline{E}(\bar{x},t) + 4\pi\overline{P}(\bar{x},t)\right]. \tag{2.8}$$

Expanding the right hand side bracket and collecting the $\overline{E}(\bar{x},t)$ terms onto the right hand side yields,

$$\nabla \times \nabla \times \overline{E}(\bar{x},t) + \frac{1}{c^2}\frac{\partial^2}{\partial t^2}\overline{E}(\bar{x},t) = \frac{4\pi}{c^2}\overline{P}(\bar{x},t). \tag{2.9}$$

The vector identity $\nabla \times \nabla \times A = \nabla(\nabla \cdot A) - \nabla^2 A$ can now be applied to the first term in Eq. (2.9) where the assumption that the first term, $\nabla(\nabla \cdot A)$, is much smaller than the second term, $\nabla^2 A$, which is therefore neglected is applied. This then leaves Eq. (2.9) as,

$$-\nabla^2\overline{E}(\bar{x},t) + \frac{1}{c^2}\frac{\partial^2}{\partial t^2}\overline{E}(\bar{x},t) = \frac{4\pi}{c^2}\overline{P}(\bar{x},t). \tag{2.10}$$

In order to study the non-linear optical effects $\overline{P}$ is usually split into its linear and non-linear components, where $\overline{P} = \overline{P}^{(1)} + \overline{P}^{NL}$. $\overline{D}$ can also be split into its same linear and non-linear components. Using these definitions Eq. (2.10) becomes,

$$-\nabla^2\overline{E}(\overline{x},t) + \frac{\epsilon}{c^2}\frac{\partial^2}{\partial t^2}\overline{E}(\overline{x},t) = \frac{4\pi}{c}\overline{P}^{NL}(\overline{x},t), \tag{2.11}$$

where ϵ is the permittivity of the material through which the wave is propagating. From Eq. (2.11) it is possible to see how the non-linear polarisation acts as a source term for the generation of travelling waves. It is also possible to see how by setting the non-linear polarisation term to zero the solution to Eq. (2.11) takes the form of a propagating electromagnetic field with velocity $\frac{c}{\sqrt{\epsilon_0}}$ which is consistent with Maxwell's equations.

Currently Eq. (2.11) gives the wave equation with the nonlinear source term in the time domain. By applying the Fourier transform to $\overline{E}(\overline{x},t)$ and $\overline{P}^{NL}(\overline{x},t)$ it is possible to convert this into a wave equation with a nonlinear source term in the frequency domain

$$-\nabla^2\overline{E}(\overline{x},\omega) - \frac{\omega_n^2\epsilon(\omega_n)}{c^2}\overline{E}(\overline{x},\omega) = \frac{4\pi\omega_n^2}{c^2}\overline{P}^{NL}(\overline{x},\omega). \tag{2.12}$$

2.2 Non-linear Polarisation

The polarisation vector, $\overline{P}$, is a localised quantity that acts as a source term in the non-linear wave equation [2]. It is a measure of the dielectric polarisation density, with units of dipole moment per unit volume. The polarisation vector can be written as a Taylor series expansion,

$$\overline{P}(\overline{x},t) = \epsilon_0\left(\chi^{(1)}\overline{E}(\overline{x},t) + \chi^{(2)}\overline{E}(\overline{x},t)^2 + \chi^{(3)}\overline{E}(\overline{x},t)^3 + \ldots\right), \tag{2.13}$$

where $\overline{E}$ is the input electric field and $\chi^{(n)}$ are the n^{th} order susceptibilities which are properties of the material in which the interaction is taking place. For the process of terahertz generation within non-linear optical materials the second order non-linear susceptibility tends to dominate and so it is possible to write

$$\overline{P}(\overline{x},t) = \overline{P}^{(1)}(\overline{x},t) + \overline{P}^{(2)}(\overline{x},t). \tag{2.14}$$

Given the expression

$$\overline{P}^{(2)}(\overline{x},t) = \chi^{(2)}\overline{E}^2(\overline{x},t), \tag{2.15}$$

it is possible to express the generated second order polarisation term in the frequency domain by taking the Fourier transform of both $\overline{P}^{(2)}(\overline{x},t)$ and $\overline{E}^{2}(\overline{x},t)$ such that

$$\overline{P}^{(2)}(\overline{x},\omega)=\chi^{(2)}\int_{-\infty}^{\infty}\overline{E}(\overline{x},\Omega)\overline{E}(\overline{x},\omega-\Omega)d\Omega. \tag{2.16}$$

This now shows how the generated polarisation term in the frequency domain is the convolution of the optical input field.

2.3 Terahertz Generation

The term terahertz radiation generally refers to electromagnetic radiation that exists at frequencies within the range 0.1×10^{12} to 10×10^{12} Hz. The temporal properties of pulsed radiation within this frequency range make it ideal for the application to modulate the energy of relativistic particles. The generation of such radiation therefore is a key part of this work. Different generation techniques enable the possibility of tuning different physical properties of any generated terahertz radiation, each generation technique having its own individual positive points and difficulties. Within this section the different generation techniques relevant to this project is discussed. The theory behind how each method generates terahertz radiation is explained along with the positive and negative points related to each method with respect to the end goals of this project.

2.3.1 Optical Terahertz Generation

The generation of terahertz radiation within non-linear crystals is commonplace in many applications that use terahertz radiation. The physical process behind this generation technique is known as difference frequency mixing, or in certain special cases optical rectification. Optical rectification involves the non-linear reaction of a material to incident optical laser radiation. These generation techniques are second order non-linear effects and therefore can be described by the second order polarisation term [3],

$$\overline{P}_{3}^{(2)}(\overline{x},\omega)=\chi^{(2)}\overline{E}_{1}(\overline{x},\omega)*\overline{E}_{2}(\overline{x},\omega) \tag{2.17}$$

The generation of terahertz radiation relies on the process of difference frequency mixing such that

$$\overline{P}_3(\overline{x},\omega) = \chi^{(2)}\overline{E}_1(\overline{x},\omega)\overline{E}_2^*(\overline{x},\omega). \tag{2.18}$$

By defining $\overline{E}_1(\overline{x},\omega)$ and $\overline{E}_2^*(\overline{x},\omega)$ as,

$$\overline{E}_1(z,\omega) = A_1 e^{i(k_1 z)}, \tag{2.19}$$

$$\overline{E}_2^*(z,\omega) = A_2^* e^{-i(k_2 z)}. \tag{2.20}$$

Now using these expressions for E_1 and E_2 and placing them into Eq. (2.18) it is possible to obtain an expression of the form,

$$\overline{P}_3(\omega_3) = 2\chi^{(2)} A_1 A_2^* e^{i(k_1 - k_2)z}. \tag{2.21}$$

If the wave generated by polarisation term $P_3(\omega_3)$ is a travelling wave in the $+z$ direction then it should also be possible to express it as

$$\overline{E}_3(z,\omega_3) = A_3 e^{i(k_3 z)}. \tag{2.22}$$

Now by placing Eqs. (2.21) and (2.22) into the non-linear wave equation, Eq. (2.12),

$$\left[-\nabla^2 A_3 - 2ik_3\nabla A_3 + k_3^2 A_3 - \frac{\omega_3^2\epsilon(\omega_3)}{c^2}A_3\right]e^{i(k_3 z)} = \frac{8\pi\omega_3^2}{c^2}\chi^{(2)} A_1 A_2^* e^{i[(k_1 - k_2)z]}. \tag{2.23}$$

Using the definition that $k_i = \frac{\sqrt{\epsilon(\omega_i)}\omega_i}{c}$ it is possible to see how the third and fourth terms within the first brackets cancel each other out. Also by defining the direction of propagation to only be allowed in the $+z$ direction it is possible to say $\nabla \approx \frac{\partial}{\partial z}$. The temporal term within the exponentials can also be cancelled from both sides and the exponential term can be dropped such that Eq. (2.23) now becomes,

$$\left[-\frac{\partial^2}{\partial z^2}A_3 - 2ik_3\frac{\partial}{\partial z}A_3\right]e^{ik_3 z} = \frac{8\pi\omega_3^2}{c^2}\chi^{(2)} A_1 A_2^* e^{i(k_1 - k_2)z}. \tag{2.24}$$

A further approximation can now be made to this expression which is commonly known as the slowly varying envelope approximation (SVEA). The SVEA is valid for cases where the envelope of the pulse varies on larger lengths scales than the wavelength of the radiation. This approximation makes the assumption that the second order differential is much smaller than the first order differential i.e. in this case,

$$\left|\frac{\partial^2}{\partial z^2}A_3\right| \ll \left|k_3\frac{\partial}{\partial z}A_3\right|. \tag{2.25}$$

If this approximation is made and applied to the current wave equation expression then the first term in Eq. (2.24) can be neglected and Eq. (2.24) becomes,

$$\frac{\partial}{\partial z}A_3 = \frac{(i^2)8\pi\omega_3^2}{2ik_3c^2}\chi^{(2)}A_1A_2^*\frac{e^{i(k_1-k_2)z}}{e^{ik_3z}}, \tag{2.26}$$

which simplifies to

$$\frac{\partial}{\partial z}A_3 = \frac{i4\pi\omega_3}{c}\chi^{(2)}A_1A_2e^{i\Delta kz}, \tag{2.27}$$

where $\Delta k = k_1 - k_2 - k_3$ and is commonly called the wave vector mismatch. In order to obtain an expression such that A_3 is isolated the integral over z is performed on the right hand side such that Eq. (2.27) becomes

$$A_3 = \frac{i4\pi\omega_3}{c}\chi^{(2)}A_1A_2^*\int_0^L e^{i\Delta kz}dz, \tag{2.28}$$

where L represents the interaction length which is typically confined to the thickness of the non-linear material in which the interaction is taking place. Performing this integral leaves,

$$A_3 = \frac{i4\pi\omega_3}{c}\chi^{(2)}A_1A_2^*\left(\frac{e^{i\Delta kL}-1}{i\Delta k}\right). \tag{2.29}$$

It is common practice to analyse the output of the newly generated propagating wave in terms of its intensity which can be defined in terms of A_i as,

$$I_i = \frac{n_ic}{2\pi}|A_i|^2, \tag{2.30}$$

where the index i denotes the wave either 1, 2 or 3. Using this definition and applying it to Eq. (2.29) it is possible to write,

$$I_3 = \frac{n_3c}{2\pi}\frac{16\pi^2\omega_3^2}{c^2}\chi^{(2)^2}|A_1|^2|A_2^*|^2\left|\frac{e^{i\Delta kL}-1}{\Delta k}\right|^2. \tag{2.31}$$

The squared modulus can be re-expressed as a sinc function, described in Appendix A.1, such that Eq. (2.31) now becomes,

$$I_3 = \frac{n_38\pi\omega_3^2}{c}\chi^{(2)^2}I_1I_2\,\mathrm{sinc}^2\left(\frac{\Delta kL}{2}\right). \tag{2.32}$$

It can now be seen that the intensity of the newly generated wave is dependent upon the square of the non-linear material property $\chi^{(2)}$, and is linearly dependent

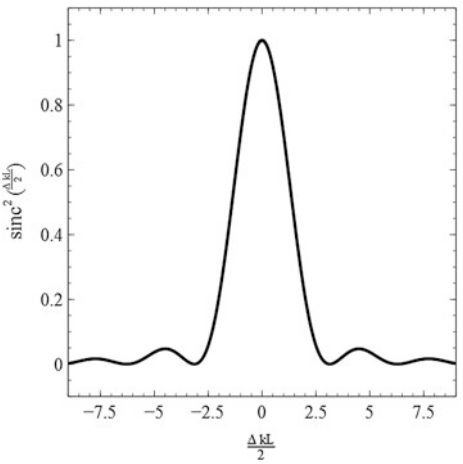

Fig. 2.1 $\sin c^2\left(\frac{\Delta kL}{2}\right)$ plotted as a function of $\frac{\Delta kL}{2}$ which represents the phase matching effects on the efficiency of difference-frequency generation

upon the product of the two input intensities I_1 and I_2. Currently this expression describes two monochromatic beams producing a third monochromatic beam with the frequency given by the difference in the input beam frequencies. This however can also be expanded such that only one input beam is present and both the input frequencies are contained within this one input beam. In this case the input beam must be have a large bandwidth such that the difference in frequencies contained within the beam are large enough to propagate. When this is true I_1 and I_2 can be thought of as different frequency components of the same beam. It can also be seen in Eq. (2.32) that the phase mismatch, described by Δk, is completely confined to the last sinc term. This phase mismatch can be thought of as an efficiency multiplier which physically limits the interaction length of the process. As can be seen in Fig. 2.1 which shows the phase mismatch term plotted as a function of efficiency, $\sin c^2\left(\frac{\Delta kL}{2}\right)$, the most efficient generation occurs when $\frac{\Delta kL}{2} = 0$. This can only be true when either Δk or L is zero, and since the non-linear interaction material thickness is required to be non-zero by definition Δk must therefore be zero to obtain a perfectly phase matched condition. Remembering the definition of $\Delta k = k_1 - k_2 - k_3$, it is often difficult to obtain perfect phase matching in any physical process, because the refractive index of materials generally increases as a function of frequency. For $\Delta k = 0$ to be true the following must also,

$$k_3 = k_1 - k_2 \tag{2.33}$$

which can also be expressed as,

$$n_3\omega_3 = n_1\omega_1 - n_2\omega_2, \tag{2.34}$$

where $\omega_3 \ll \omega_2 < \omega_1$ and therefore,

$$n_3 - n_2 = \frac{(n_1 - n_2)\omega_1}{\omega_3}. \tag{2.35}$$

Notice for materials that display normal dispersion $n_3 \gg n_2$ and so the left hand side must be negative, however $n_1 > n_2$ and so the right hand side must be positive. In the absence of negative angular frequencies Eq. (2.35) therefore implies that perfect phase matching cannot occur in materials which have normal dispersion around the frequency region of the interaction. It is however possible to obtain phase matching using Eq. (2.35) in materials that display anomalous phase matching, that is to say the refractive index decreases as a function of frequency. Another common way to obtain phase matching is to make use of the birefringence of a material, which enables electric fields polarised along different crystal axes to experience different refractive indices [2].

This condition adds a new limit onto the type of material that can be used for the generation of terahertz radiation within non-linear optical crystals; as well as having a strong $\chi^{(2)}$ term the crystal must also be birefringent such that it is possible to obtain phase matching between the pump laser and terahertz radiation.

2.3.1.1 Generation Within Zinc Telluride

Within this section an example of terahertz generation using a femtosecond laser within a zinc telluride (ZnTe) crystal is presented [4]. For this case the second order non-linear polarisation term can be re-written in the frequency domain as,

$$P_i^{(2)}(\Omega) = \sum_{j,k} \epsilon_0 \chi_{ijk}^{(2)} E_i(\omega) E_k^*(\Omega - \omega), \tag{2.36}$$

where Ω is the frequency of the generated wave and ω is the optical frequency. The indices ijk represent axes that lie along a Cartesian axis grid in the frame of the crystal. If Kleinman symmetry holds, which states that if the frequencies involved are much smaller than the lowest resonance frequency of the material system then the nonlinear susceptibility tensor is no longer dependent on frequency, then the indices must also be permutable [2]. Such a symmetry condition is true for the generation of terahertz radiation within ZnTe and so contracted notation can be used to help simplify the form of Eq. (2.36). Contracted notation invokes a new index l which combines the two last indices jk into a single index [2, 4]. The relation between l and jk can be seen in Table 2.1.

This then enables $\chi_{ijk}^{(2)}$ to be redefined as d_{il} where,

$$d_{il} = \frac{1}{2}\chi_{ijk}^{(2)}, \tag{2.37}$$

Table 2.1 Conversion between standard and contracted notation [2]

jk	11	22	33	23,32	31,13	12,21
l	1	2	3	4	5	6

and enables d_{il} to be expressed as a 3×6 matrix:

$$d_{il} = \begin{bmatrix} d_{11} & d_{12} & d_{13} & d_{14} & d_{15} & d_{16} \\ d_{21} & d_{22} & d_{23} & d_{24} & d_{25} & d_{26} \\ d_{31} & d_{32} & d_{33} & d_{34} & d_{35} & d_{36} \end{bmatrix}. \tag{2.38}$$

The generation of the polarisation term can now be written as,

$$\begin{bmatrix} P_x \\ P_y \\ P_z \end{bmatrix} = 2\epsilon_0 \begin{bmatrix} d_{11} & d_{12} & d_{13} & d_{14} & d_{15} & d_{16} \\ d_{21} & d_{22} & d_{23} & d_{24} & d_{25} & d_{26} \\ d_{31} & d_{32} & d_{33} & d_{34} & d_{35} & d_{36} \end{bmatrix} \times \begin{bmatrix} E_x E_x^* \\ E_y E_y^* \\ E_z E_z^* \\ 2E_y E_z^* \\ 2E_z E_x^* \\ 2E_x E_y^* \end{bmatrix}. \tag{2.39}$$

ZnTe is a crystal which exists within the $\bar{4}3m$ point group. This defines the symmetries which exist within the crystal structure and enables the d_{il} tensor to be simplified to,

$$d_{il} = \begin{bmatrix} 0 & 0 & 0 & d_{14} & 0 & 0 \\ 0 & 0 & 0 & 0 & d_{25} & 0 \\ 0 & 0 & 0 & 0 & 0 & d_{36} \end{bmatrix}, \tag{2.40}$$

where $d_{14} = d_{25} = d_{36}$. The electric field of the pump laser can be defined as,

$$E = E_0 \begin{bmatrix} \sin(\theta)\cos(\phi) \\ \sin(\theta)\sin(\theta) \\ \cos(\theta) \end{bmatrix}, \tag{2.41}$$

where θ is the polar angle and ϕ is the azimuthal angle and using these definitions and simplifications Eq. (2.36) now becomes,

$$\begin{bmatrix} P_x \\ P_y \\ P_z \end{bmatrix} = 2\epsilon_0 d_{14} E_0^2 \begin{bmatrix} 0 & 0 & 0 & 1 & 0 & 0 \\ 0 & 0 & 0 & 0 & 1 & 0 \\ 0 & 0 & 0 & 0 & 0 & 1 \end{bmatrix} \times \begin{bmatrix} \sin^2(\theta)\cos^2(\phi) \\ \sin^2(\theta)\sin^2(\phi) \\ \cos^2(\theta) \\ 2\sin(\theta)\cos(\theta)\sin(\phi) \\ 2\sin(\theta)\cos(\theta)\cos(\phi) \\ 2\sin^2(\theta)\sin(\phi)\cos(\phi) \end{bmatrix}, \tag{2.42}$$

which when simplified gives,

$$\begin{bmatrix} P_x \\ P_y \\ P_z \end{bmatrix} = 4\epsilon_0 d_{14} E_0^2 \sin(\theta) \begin{bmatrix} \cos(\theta)\sin(\phi) \\ \cos(\theta)\sin(\phi) \\ \sin(\theta)\sin(\phi)\cos(\phi) \end{bmatrix}. \tag{2.43}$$

As in Sect. 2.3.1 it is now common to express this in terms of an intensity. Using the same definition as given by Eq. (2.30) this now becomes,

$$I = \frac{2nc\epsilon_0^2 d_{41}^2 E_0^4 \sin^2(\theta)}{\pi} \left[4\cos^2(\theta) + \sin^2(\theta)\sin^2(2\phi)\right]. \tag{2.44}$$

Noticing that the only component of Eq. (2.44) that contains a ϕ dependence is the $\sin^2(2\phi)$ term it is clear that the intensity of the generated terahertz wave is maximised when this term is maximised. This is true when $\phi = n\frac{\pi}{4}$ where n is an odd integer, as can be seen from . Setting ϕ to $\frac{\pi}{4}$ enables Eq. (2.44) to be written such that it only depends upon θ,

$$I = \frac{2nc\epsilon_0^2 d_{41}^2 E_0^4}{\pi} \sin^2(\theta)\left[4 - 3\sin^2(\theta)\right]. \tag{2.45}$$

Given that θ is the polar angle, that being the angle between the [110] crystal axis and the laser polarisation, it can be seen from Eq. (2.45) and Fig. 2.3 the generated intensity is maximised when $\theta = 54°$. Therefore optimal terahertz generation will occur when the pump beam is polarised at 54° to the [110] crystal edge when incident upon the $(\overline{1}10)$ crystal surface. This can be said to be true for any crystal that has the same crystal symmetries as ZnTe, such as gallium phosphide (GaP). However for crystals that exhibit different symmetry properties, such as lithium niobate ($LiNbO_3$) this expression can change drastically. These different forms will be discussed in further chapters when relevant (Fig. 2.2).

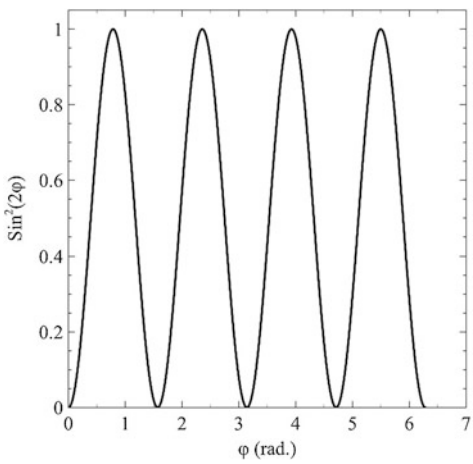

Fig. 2.2 Plot showing the generated terahertz dependence on the angle ϕ

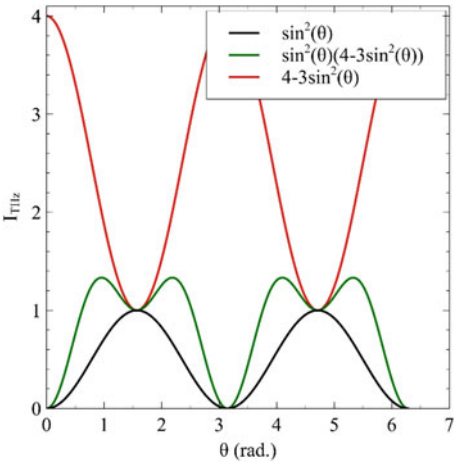

Fig. 2.3 Generated terahertz intensity as a function of the polar angle, θ

2.3.1.2 Generation Within Magnesium-Oxide-Doped Stoichiometric Lithium Niobate

Generation of terahertz radiation within magnesium-oxide-doped stoichiometric lithium niobate (MgO:SLN) differs from generation within ZnTe and GaP due to the different crystal properties, specifically symmetries. To investigate the generation within MgO:SLN it is possible to start with,

$$\begin{bmatrix} P_x \\ P_y \\ P_z \end{bmatrix} = 2\epsilon_0 \begin{bmatrix} d_{11} & d_{12} & d_{13} & d_{14} & d_{15} & d_{16} \\ d_{21} & d_{22} & d_{23} & d_{24} & d_{25} & d_{26} \\ d_{31} & d_{32} & d_{33} & d_{34} & d_{35} & d_{36} \end{bmatrix} \times \begin{bmatrix} E_x E_x^* \\ E_y E_y^* \\ E_z E_z^* \\ 2E_y E_z^* \\ 2E_z E_x^* \\ 2E_x E_y^* \end{bmatrix}, \tag{2.46}$$

to which the relevant crystal symmetries are applied. MgO:SLN has a 3 m crystal symmetry which means the d_{il} matrix can be expressed as,

$$d_{il} = \begin{bmatrix} 0 & 0 & 0 & 0 & d_{31} & d_{21} \\ d_{21} & -d_{21} & 0 & d_{31} & 0 & 0 \\ d_{31} & d_{31} & d_{33} & 0 & 0 & 0 \end{bmatrix}. \tag{2.47}$$

Experimental measurements of the non-zero values d_{21}, d_{31} and d_{33} have shown that d_{33} is much larger than d_{21} and d_{31} [2]. It is therefore possible to further simplify Eq. (2.47) by setting both $d_{21} \approx 0$ and $d_{31} \approx 0$, leaving,

$$d_{il} = \begin{bmatrix} 0 & 0 & 0 & 0 & 0 & 0 \\ 0 & 0 & 0 & 0 & 0 & 0 \\ 0 & 0 & d_{33} & 0 & 0 & 0 \end{bmatrix}. \tag{2.48}$$

Then, by using Eq. (2.48) and placing it into Eq. (2.46) it is possible to arrive at

$$\begin{bmatrix} P_x \\ P_y \\ P_z \end{bmatrix} = 2\epsilon_0 \begin{bmatrix} 0 & 0 & 0 & 0 & 0 & 0 \\ 0 & 0 & 0 & 0 & 0 & 0 \\ 0 & 0 & d_{33} & 0 & 0 & 0 \end{bmatrix} \times \begin{bmatrix} E_x E_x^* \\ E_y E_y^* \\ E_z E_z^* \\ 2E_y E_z^* \\ 2E_z E_x^* \\ 2E_x E_y^* \end{bmatrix}, \tag{2.49}$$

which when simplified gives,

$$\begin{bmatrix} P_x \\ P_y \\ P_z \end{bmatrix} = 2\epsilon_0 d_{33} \begin{bmatrix} 0 \\ 0 \\ E_z E_z^* \end{bmatrix}. \tag{2.50}$$

This is an important result as it states that in order to generate terahertz radiation the input beams must be linearly polarised along the z axis. It also states that any generated terahertz radiation will also be polarised along the same z axis.

The above result, Eq. (2.50), provides information regarding the required polarisation of the pump laser as well as the polarisation of the generated 2nd order polarisation term, $\overline{P}$. To investigate how this polarisation term forms a propagating wave the refractive indices at both the optical pump wavelength and the generated terahertz radiation wavelength must be obtained in order to perform a phase-matching calculation. The refractive index of MgO:SLN at 800 nm is 2.25 and at 0.1 mm is 4.96. The large difference in refractive indices means that the generated non-linear polarisation produces radiation which coherently adds to form a Cherenkov cone which trails the optical pump [5]. The angle of this cone defined as θ in Fig. 2.4 can be expressed as a function of the generated terahertz radiation refractive index and the optical pump refractive index through

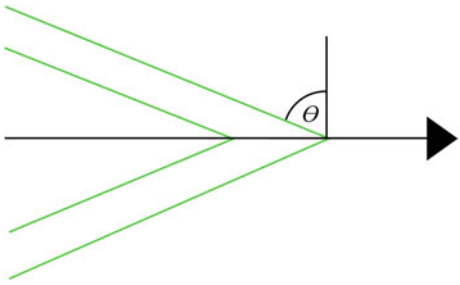

Fig. 2.4 Cherenkov cone formed inside MgO:SLN by an 800 nm laser beam (*black*). *Green lines* represent the generated wave fronts of the terahertz radiation at an angle of θ to the wave fronts of the optical generation beam (color figure online)

$$\tan(\theta) = -\frac{n_{THz}}{n_{opt}}\omega\frac{d\Theta}{d\omega}, \tag{2.51}$$

where n_{THz} is the terahertz refractive index of 4.96, n_{opt} is the optical refractive index of 2.25, θ is the angle of tilt and $\frac{d\Theta}{d\omega}$ represents the angular dispersion. This expression can be expressed solely as a function of the two refractive indices as,

$$\theta = \cos^{-1}\left(\frac{n_{opt}}{n_{THz}}\right). \tag{2.52}$$

When combined with the correct refractive index values a Cherenkov cone angle of 63.02° is obtained [6]. In order to obtain efficient and scalable generation the pulse front of the pump laser should be matched to this angle so that the generated radiation coherently adds to form a propagating pulse. This feature is known as a pulse front tilt (PFT) and is commonly produced via grating—imaging optical systems. When radiation undergoes dispersion, such as when it is incident upon a grating, different wavelengths travel different paths. This spectral dispersion means that the radiation rapidly becomes larger as the different spectral components become spatially separated. However in the near field of such a dispersive medium, whilst all components of the radiation are spatially overlapped, the difference in path length travelled by each spectral component gives rise to a propagating beam with a wave front that is tilted at a non-orthogonal angle to the propagation direction. An imaging system can then be used to image the plane at which the tilt exists to another more distant plane, thus providing a far field pulse front tilt, as can be seen in Fig. 2.5.

Equation (2.52) describes the tilt required inside the MgO:SLN for optimal generation to occur; however the actual tilt is generated externally by a lens and grating combination. Due to the effective length changes of the generation radiation caused by the refractive index of the material and any magnification caused by the imaging system the tilt generated externally will be different to the internal tilt. The pulse front tilt generated by a grating can be expressed as,

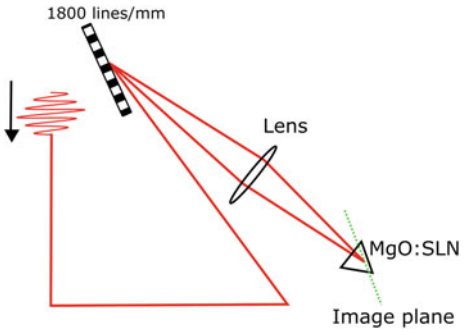

Fig. 2.5 Schematic diagram showing the collection and transport of optical radiation with a pulse-front-tilt from a grating to the image plane situated within a MgO:SLN crystal (color figure online)

$$\theta_g = \tan^{-1}\left(\frac{m\lambda}{d\ \cos(\phi)}\right). \tag{2.53}$$

In Eq. (2.53) θ_g represents the tilt generated by the grating, m is the diffraction order, λ is the wavelength of the optical pump, d is the number of groves per mm on the grating and ϕ is the diffraction angle which describes the angle at which the output radiation leaves the grating. Using geometry it is possible to convert the tilt angle required inside the crystal to an external tilt angle, which is the angle that would need to be generated by the grating. This conversion takes the form,

$$\tan(\theta_g) = n_{opt}\beta\ \tan(\theta), \tag{2.54}$$

where n is the refractive index of the material and β is the magnification of the pump beam induced by the imaging system. Therefore by combing Eq. (2.53) and Eq. (2.54) it is possible to express the required internal tilt as a function of optical system parameters,

$$\theta = \tan^{-1}\left[\frac{1}{n_{opt}\beta}\left(\frac{m\lambda}{d\ \cos(\phi)}\right)\right]. \tag{2.55}$$

As the required internal tilt is fixed at approximately 63° it is now possible to design an optical system that will provide the required tilt.

This tilt geometry dictates the physical shape of the crystal as the input surface is required to be perpendicular to the optical input beam and the output surface is required to be perpendicular to the generated terahertz radiation so as to reduce reflections in both cases. The geometry of the crystal can be seen in Fig. 2.6; here the red line denotes the optical input radiation and the green lines represent the generated radiation output. Angles θ_g and θ represent the external and internal angles respectively. In Fig. 2.6 the z-axis of the crystal is orientated perpendicular to the page and thus according to Eq. (2.50) the polarisation of both beams is required to be orientated along the same axis.

The terahertz radiation that is generated along the output surface of the $LiNbO_3$ is not produced with a uniform profile. This is due to three properties of the

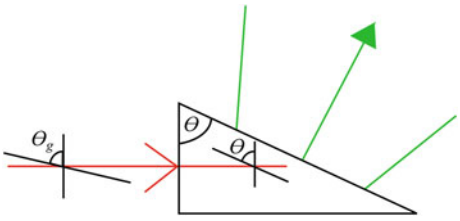

Fig. 2.6 Required geometrical shape of the MgO:SLN crystal, the *red line* denotes the optical pump beam, the *green lines* denote the generated terahertz radiation. The angle θ represents the internal tilt angle and angle θ_g represents the external tilt angle (color figure online)

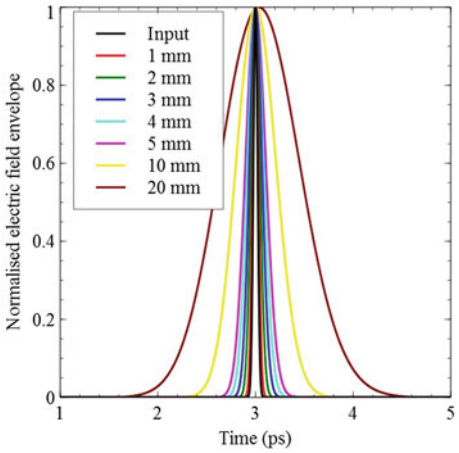

Fig. 2.7 Simulation showing the temporal dispersion induced onto an 800 nm optical pump laser passing through various thicknesses of MgO:SLN crystal

generation technique, firstly the spatial profile of the pump beam which typically does not have a uniform intensity profile. The second property relates to the geometry of the generation system. As can be seen from Fig. 2.6 different parts of the pump beam travel through different lengths of the $LiNbO_3$ crystal, therefore experiencing a different effective crystal length. The third factor which affects the terahertz profile on the output surface relates to the dispersion of the pump beam within the $LiNbO_3$ crystal. As $LiNbO_3$ is a highly dispersive medium within the 800 nm wavelength range and due to the spatially varying effective crystal thickness the pump beam has a transversely varying temporal profile. The effects of the dispersion on the temporal profile of the pump laser can been seen in Figs. 2.7 and 2.8. The FWHM values of the temporal profile in Fig. 2.8 is found by first fitting a Gaussian to the temporal profile and then using the FWHM value given from the Gaussian equation. This can cause errors if the pump profile does not have a

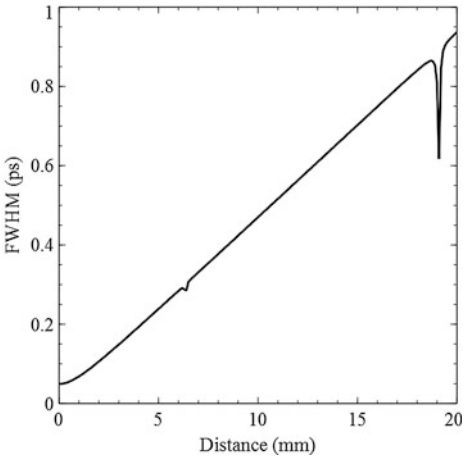

Fig. 2.8 Simulated FWHM temporal duration of a 50 fs input laser of wavelength 800 nm as a function of propagation distance through MgO:SLN

Gaussian shape. These errors manifest within Fig. 2.8 at around 6 and 19 mm and can be seen as the sharp negative peaks. Here a 50 fs 800 nm pulse is propagated through varying thicknesses of MgO:SLN. As can be seen the pulse width is broadened in time with the FWHM approaching 1 ps after 20 mm propagation. This can have a big effect on the generation efficiency as one side of the pulse will only propagate through less than 1 mm of MgO:SLN whereas the other side of the pulse could travel through up to 5 mm of MgO:SLN.

2.4 Terahertz Detection

Terahertz detection is typically more difficult than the detection of optical radiation. This is mainly due to the low photon energy of terahertz radiation. This low photon energy makes standard semiconductor-based detectors impractical as they rely on the photo-excitation of charge carriers from the valence band into the conduction band. This requires the energy of the photon to be greater than the band gap of the semiconductor and currently semiconductors used in detectors have band gaps larger than the terahertz photon energy. Due to this other forms of detection are required. These other forms typically fall into two categories, thermal and electro-optic. Within this section both of these detection forms are explained and investigated including their positive and negative attributes and typical uses.

2.4.1 Thermal Terahertz Detectors

Thermal detectors, as the name suggests, rely on the thermal properties of a material to detect radiation. When radiation is absorbed by a material energy is transferred from the radiation to the material, and as the material receives energy it heats up. Whilst thermal detectors are able to detect radiation in the terahertz frequency range they do have limitations. These limitations typically include high background noise, as they are sensitive to thermal radiation and a change in the surrounding temperature will cause a change in the background level. Also all forms of radiation transfer thermal energy to the detector and therefore all radiation absorbed by the detector contributes towards the outputted signal. The response times of thermal detectors is also typically very slow, on the μs time scales. This makes them impractical for applications that use ultrafast terahertz pulses, on the 100's fs timescale, to perform measurements that require good time resolution. These applications include terahertz waveform analysis and pump-probe style spectroscopic experiments. Due to their workings these detectors tend to be large in spatial size and thus are not suitable for experiments that require good spatial resolution;

however this aspect has seen progress with the advent of micro-bolometer arrays. These micro-bolometer arrays have been shown to produce terahertz images with spatial resolutions down to 50 μm [7]. There are three common thermal terahertz detectors which are the bolometer, Golay cell and pyro electric detectors.

2.4.1.1 Bolometer

A bolometer is a device which measures the power of incident radiation via the thermal transfer of energy to a material which has a temperature dependent electric resistance. Typically bolometers consist of an absorbing material, a transfer material and a thermal reservoir. Radiation is incident upon the absorbing material causing it to absorb energy from the radiation and heat up. This material is attached to the thermal reservoir via the transfer material. The thermal reservoir is kept at a constant low temperature. Therefore as the absorbing material heats up a temperature difference between the absorbing material and thermal reservoir is formed and heat energy therefore flows through the transfer material towards to thermal reservoir forming a thermal equilibrium. The transfer material therefore experiences a time dependent thermal change. The transfer material is typically chosen such that its resistance is highly dependent upon temperature. Therefore this temporally dependent thermal change is measured by monitoring the resistance of the transfer material.

To make the bolometer sensitive the temperature of the thermal reservoir must be kept cold and constant. Such bolometers are typically contained within a cooling chamber which contains liquid helium or liquid nitrogen. This typically limits their response time to the μs range as it is limited by the flow of thermal energy from the absorber to the thermal reservoir. They can however be extremely sensitive with commercially available units able to detect less than 1 nJ per of terahertz pulse energy. This makes bolometers the most sensitive type of thermal detectors for terahertz radiation [8, 9].

2.4.1.2 Golay Cell

A Golay cell is a thermal detector that uses the expansion and contraction of a material due to its temperature change. Typically it consists of a gas-filled enclosure with an absorbing material inside. As the absorbing material receives energy from the incident radiation it heats up, and this thermal energy is then dissipated to the surrounding gas. As the gas heats up it expands causing a membrane in the wall of the enclosure to expand and contact. This expansion and contraction is then detected either using an audio detector such as a microphone or a laser which monitors the surface position. The response time of a Golay cell is typically on the order of 10's of ms and is one of the slowest thermal detectors. However it is still sensitive and able to detect terahertz radiation with pulse energies down to the nJ

level. The sensitivity of a Golay cell is also not strongly dependent upon frequency, thus giving the Golay cell a very flat response over a broad range of frequencies. This makes the Golay cell good when trying to accurately calculate the pulse energy of an ultrafast broadband terahertz pulse [10].

2.4.1.3 Pyroelectric Detector

Pyroelectric detectors are the third type of commonly used thermal detector. They generally consist of a crystalline lithium tantalate material (CLT), an absorbing material and a set of electrodes. The radiation falls onto the absorbing material which converts the radiation energy into thermal energy. This thermal energy is then transferred onto the CLT. Crystalline lithium tantalate is a ferroelectric material and thus exhibits spontaneous electrical polarisation when below the Curie temperature. When the temperature of the CLT is altered the electrical polarisation rotates. Therefore by using electrodes to read of the electrical polarisation only in one axis the temperature change can be monitored. As the temperature change is as a direct result of the incident radiation heating up the absorbing material the signal produced by the electrodes is directly proportional to the incident radiation power. Again as with the other thermal detectors pyroelectric detectors have slow response times on the 100's μs timescale. However they do have a flat response to frequency which is only limited by the absorbing material. They are also able to be made into very small devices, on the 100's μm scale, providing the ability for good spatial resolution [11].

2.4.2 Electro-Optic Detection

Electro-optic detection is a common form of terahertz radiation detection. It involves mixing a near-infrared (NIR) laser with the terahertz radiation inside a non-linear optical material. The same, but reverse, non-linear physical process as used in the non-linear optical generation of terahertz radiation then causes information contained within the terahertz radiation to be transferred into the NIR laser pulse. This can then be detected using standard semiconductor style detectors.

The physics involved in transferring information from the terahertz electric field into the optical detection laser is the same as is involved in the optical generation of terahertz radiation as described in Sect. 2.3.1. Commonly-used detection crystals are ZnTe and GaP both of which display the same crystal structure and symmetry components [12]. For electro-optic detection however it is easier to think of the terahertz radiation as changing the relative permittivity of the material, effectively changing the refractive index of the material. The optical probe beam will therefore experience this change in refractive index and propagate accordingly [13–16].

The electric displacement vector can be linked to the electric field via

$$\begin{bmatrix} D_x \\ D_y \\ D_z \end{bmatrix} = \epsilon_0 \begin{bmatrix} \epsilon_x & 0 & 0 \\ 0 & \epsilon_y & 0 \\ 0 & 0 & \epsilon_z \end{bmatrix} \begin{bmatrix} E_x \\ E_y \\ E_z \end{bmatrix}, \tag{2.56}$$

where ϵ_n represents the square root of the refractive index along the axis n. In the case of a homogeneous material, where no birefringence is present, $\epsilon_x = \epsilon_y = \epsilon_z$. However for cases where birefringence is present $\epsilon_x \neq \epsilon_y \neq \epsilon_z$ can be true. To define a surface of constant energy density, the energy density must first be defined as $u = \frac{1}{2}\overline{E}\,\overline{D}$ [17]. Using this definition and Eq. (2.56) it is then possible to define such a surface as

$$\epsilon_0 u = \frac{D_x^2}{\epsilon_x} + \frac{D_y^2}{\epsilon_y} + \frac{D_z^2}{\epsilon_z}. \tag{2.57}$$

It is now clear that for a non-birefringent material the surface of constant energy density would take the form of a sphere and for a birefringent material it would take the form of an ellipse. Using the standard relationship between refractive index and ϵ_n, $n_n = \sqrt{\epsilon_n}$, and by defining a dimensionless vector along the direction of $\overline{D}$, $\overline{s} = \frac{\overline{D}}{\sqrt{2\epsilon_0 u}}$ it is possible to obtain the equation of the refractive index ellipsoid,

$$\frac{s_x^2}{n_x^2} + \frac{s_y^2}{n_y^2} + \frac{s_z^2}{n_y^2} = 1. \tag{2.58}$$

Now by defining a new tensor which is known as the impermeability tensor, $\overline{\overline{n}}$,

$$\overline{\overline{n}} = \overline{\epsilon}^{-1}, \tag{2.59}$$

the previous refractive index ellipsoid equation, Eq. (2.58), becomes,

$$\overline{s}\overline{\overline{n}}\overline{s} = 1. \tag{2.60}$$

Now these results can be taken and applied to a practical application such as terahertz detection in ZnTe with a 50 fs 800 nm laser beam. ZnTe has a cubic lattice structure and is isotropic. This means the impermeability tensor can be replaced by by the scalar quantity $\epsilon^{-1}\overline{I}$, where $\overline{I}$ is the identity matrix. When terahertz radiation is incident upon the ZnTe crystal the impermeability tensor becomes,

$$\overline{\overline{n}}(E_T) = \epsilon^{-1}\overline{I} + \chi^{(2)}\overline{E}_t. \tag{2.61}$$

This now converts the ellipsoid equation, Eq. (2.60), into an ellipsoid equation which depends upon the applied terahertz electric field,

$$\overline{\overline{sns}} = \sum_{i,j=x,y} \left(\epsilon^{-1} \delta_{ij} + \sum_{k=z} r_{ijk} E_{T,k} \right) s_x s_y = 1. \tag{2.62}$$

It is now possible to express this in contracted notation as previously explained in Sect. 2.3.1 and the same symmetries used for generation can be applied such that only one independent value of r_{ijk}, $r_{il} = r_{41} = r_{52} = r_{63}$, is present. This therefore enables the refractive index ellipsoid equation to be rewritten as,

$$\frac{1}{n_0^2}\left(s_x^2 + s_y^2 + s_z^2\right) + 2r_{41}\left(E_{T,x}s_y s_z + E_{T,y}s_x s_z + E_{T,z}s_x s_y\right) = 1. \tag{2.63}$$

This equation can now be transformed into the crystal axis frame. Typically ZnTe is cut in the (110) plane with both the terahertz radiation and optical probe radiation propagating perpendicular to this plane with their electric field vectors in the (110) plane. Defining a new co-ordinate system (l, m, n) with l lying along the $[\overline{1}10]$ direction and m lying along the [001] direction and allowing the terahertz radiation electric field vector to rotate around the l axis at an angle of α it is possible to express the terahertz electric field vector, $\overline{E}_T$ as,

$$\overline{E}_T = E_T \begin{bmatrix} -\cos\left(\frac{\alpha}{\sqrt{2}}\right) \\ \cos\left(\frac{\alpha}{\sqrt{2}}\right) \\ \sin(\alpha) \end{bmatrix} \tag{2.64}$$

In this geometrical setup with the ZnTe limitations applied this now leaves the refractive index ellipsoid equation as

$$\overline{sn}(E_T)\overline{s} = 1, \tag{2.65}$$

and the impermeability tensor as

$$\begin{aligned} \overline{n}(E_T) = \frac{1}{n_0^2} \begin{pmatrix} 1 & 0 & 0 \\ 0 & 1 & 0 \\ 0 & 0 & 1 \end{pmatrix} \ldots \\ + r_{41} E_T \begin{pmatrix} 0 & \sin(\alpha) & \cos\left(\frac{\alpha}{\sqrt{2}}\right) \\ \sin(\alpha) & 0 & -\cos\left(\frac{\alpha}{\sqrt{2}}\right) \\ \cos\left(\frac{\alpha}{\sqrt{2}}\right) & -\cos\left(\frac{\alpha}{\sqrt{2}}\right) & 0 \end{pmatrix}. \end{aligned} \tag{2.66}$$

The refractive index along each of the (x, y, z) axes can now be calculated using $n_n = 1/\sqrt{\lambda_n}$, where λ_n is the eigenvector which lies along either x, y or z. To calculate the eigenvectors first the eigenvalues must be calculated which are

$$\lambda_{x,y} = \frac{1}{n_0^2} - \frac{r_{41}E_T}{2}\left(\sin(\alpha) \pm \sqrt{1+3\cos^2(\alpha)}\right), \tag{2.67}$$

$$\lambda_z = \frac{1}{n_0^2} + r_{41}E_T \sin(\alpha). \tag{2.68}$$

From these the normalised eigenvectors are

$$S_{x,y} = \frac{1}{2}\sqrt{1 \pm \frac{\sin(\alpha)}{\sqrt{1+3\cos^2(\alpha)}}}\begin{bmatrix} \pm 1 \\ \mp 1 \\ \frac{2\sqrt{2}\cos(\alpha)}{\sqrt{1+3\cos^2(\alpha)+\sin(\alpha)}} \end{bmatrix}, \tag{2.69}$$

$$S_z = \frac{1}{\sqrt{2}}\begin{bmatrix} 1 \\ -1 \\ 0 \end{bmatrix}. \tag{2.70}$$

The refractive indices along each axis as a function of incident terahertz field strength are therefore,

$$n_x = n_0 + \frac{n_0^3 r_{41}E_T}{4}\left(\sin(\alpha) + \sqrt{1+3\cos^2(\alpha)}\right), \tag{2.71}$$

$$n_y = n_0 + \frac{n_0^3 r_{41}E_T}{4}\left(\sin(\alpha) - \sqrt{1+3\cos^2(\alpha)}\right), \tag{2.72}$$

$$n_z = n_0 - \frac{n_0^3 r_{41}E_T}{2}\sin(\alpha). \tag{2.73}$$

These refractive indices can be seen plotted in both the principal frame and the crystal frame in Fig. 2.9. Here both the terahertz and optical detection radiation propagate into the picture perpendicularly to both the [001] and [–110] axes. This direction has previously been denoted $S_z = \left(-\frac{1}{\sqrt{2}}, -\frac{1}{\sqrt{2}}, 0\right)$. The electric field

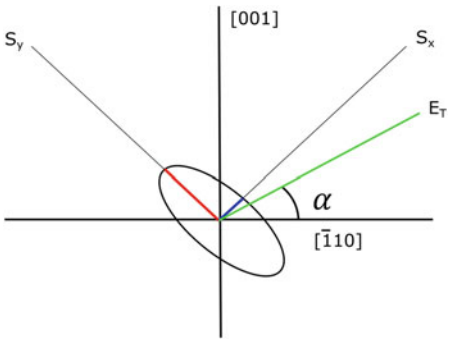

Fig. 2.9 Refractive index ellipsoid in both the crystal frame and the principal frame. n_x (*blue*) and n_y (*red*) are shown as well as the polarisation (*green*) of the applied terahertz field

vector of the optical detection radiation is fixed along the $[\bar{1}10]$ axis whilst the electric field vector of the terahertz is allowed to rotate azimuthally around [110]. The angle the terahertz electric field vector makes with the [–110] axis is denoted α in Fig. 2.9.

Taking all of the above described geometry into account the optical probe electric field experiences a phase change due to the difference in the two refractive indices, n_x and n_y of Γ, where,

$$\Gamma = \frac{\omega_o L}{c}\left(n_x - n_y\right), \tag{2.74}$$

where L is the crystal thickness and ω_o is the optical probe electric field angular frequency. Combining Eq. (2.74) with the refractive index equations described in Eqs. (2.71) and (2.72), it is possible to express the relative phase shift experienced by the optical probe as a function of applied terahertz electric field strength [18] as

$$\Gamma = \frac{\pi d}{\lambda_0} n_0^3 r_{41} E_T \sqrt{1 + 3\cos^2(\alpha)}. \tag{2.75}$$

The dependence of the relative phase shift experienced by the optical probe on the angle of the terahertz electric field orientation can be seen in Fig. 2.10. As can be seen from this figure the relative phase shift is maximised when the terahertz electric field is orientated with an α angle of 0°. This means that the maximum detectable signal will be obtained when both the optical detection electric field and the terahertz electric field are aligned with the $[\bar{1}10]$ axis.

Whilst the above describes how the optical probe is changed inside the detection crystal the information that can be extracted depends upon how the change in the

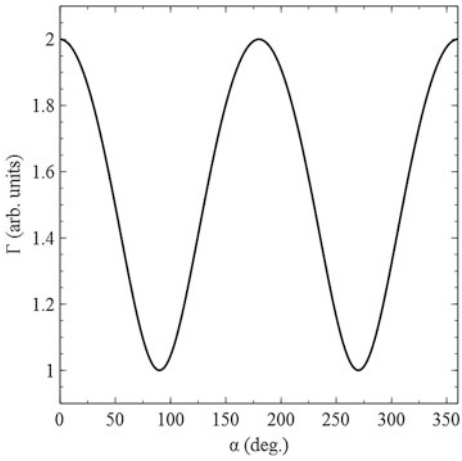

Fig. 2.10 Measured phase shift of an optical probe beam within a ZnTe detection crystal due to the presence of terahertz radiation as a function of the $[\bar{1}10]$ crystal angle α

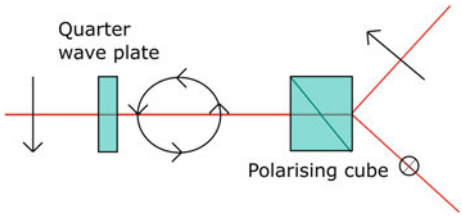

Fig. 2.11 Schematic diagram of the optical scheme for balanced detection, showing the linearly polarised input beam being converted into a circularly polarised beam and then two orthogonal linearly polarised beams

optical electric field is detected. Typically there are two main types of probe detection each enabling a different type of information regarding the terahertz field to be obtained. These two methods are balanced detection, cross-polarised detection.

2.4.2.1 Balanced Detection

Balanced detection uses a quarter wave plate, a polarising beam cube and a set of two photodiodes to convert the phase change experienced by the optical probe electric field into a difference in polarisation state. Each polarisation state is then detected by a separate photodiode. This can be seen in Fig. 2.11, where the optical probe is shown in red with the polarisation states shown in black at each part of the optical setup.

To analyse how the phase change converts to a detectable signal, Jones matrices are used to propagate the electric field through the optical components used [19]. By setting α to 0°, such that ZnTe crystal is orientated with its (110) surface aligned to the polarisation of the terahertz radiation and the optical probe laser the Jones matrix calculation for balanced detection becomes

$$\overline{E}_{out} = \overline{R}(-\phi)\overline{M}_w\overline{R}(\phi)\overline{R}(-\theta)\overline{M}_\Gamma\overline{R}(\theta)\overline{E}_{in}, \tag{2.76}$$

where $\overline{E}_{out}$ is the vector, $\begin{pmatrix} E_{x,out} \\ E_{y,out} \end{pmatrix}$, representing the output of the system, $\overline{R}(\theta)$ is a rotation matrix equal to $\begin{pmatrix} \cos(\theta) & -\sin(\theta) \\ \sin(\theta) & \cos(\theta) \end{pmatrix}$, $\overline{M}_w$ is the quarter wave plate matrix equal to $\begin{pmatrix} e^{\frac{i\pi}{4}} & 0 \\ 0 & e^{-\frac{i\pi}{4}} \end{pmatrix}$, $\overline{M}_\Gamma$ is the matrix which represents the phase rotation induced by the terahertz electric field and is equal to $\begin{pmatrix} e^{i\Gamma} & 0 \\ 0 & e^{-i\Gamma} \end{pmatrix}$ and $\overline{E}_{in}$ is the input optical detection electric field vector. The measured signal, $\Delta I/I_0$, output by a

lock-in amplifier is a measure of $\left|E_{x,out}\right|^2 - \left|E_{y,out}\right|^2$. This now allows for the measured signal to be expressed as a function of the phase rotation induced by the terahertz radiation such:

$$S = \frac{\Delta I}{I_0} = \sin(\Gamma). \tag{2.77}$$

Applying the small angle approximation and using Eq. (2.75) the following equation can be written

$$E_{THz} = \frac{\Delta I}{I_0} \frac{\lambda}{2\pi n^3 r_{41} L}, \tag{2.78}$$

where λ is the optical detection optical field wavelength, ΔI represents the change in the photodiode signals as measured by the lock-in amplifier, I_0 is 2 times the photodiode level with no terahertz radiation present (again as measured by the lock-in amplifier), n is the refractive index of the optical detection radiation inside the detection crystal, r_{41} is the electro-optic co-efficient of the detection crystal and L is the crystal thickness. Equation (2.78) represents the terahertz electric field strength inside the detection crystal. Additional factors can be added to account for losses in the terahertz radiation due to reflections and losses as well as calibration factors to account for errors in devices used. Adding these factors in (2.78) gives,

$$E_{THz} = \frac{\Delta I}{I_0} \frac{\lambda}{2\pi n^3 r_{41} L} TC, \tag{2.79}$$

where T represents the transmission coefficient of the detection material and C represents correction factors applied to account for errors in any measuring devices. This equation, Eq. (2.79), now describes the terahertz electric field strength external to the detection crystal as measured by balanced detection [20].

2.4.2.2 Crossed-Polarised Detection

Crossed-polarised detection uses similar optics to the previously described balanced detection, however the quarter wave plate is replaced with a half wave plate. The half wave plate is set such that in the absence of terahertz radiation the probe beam is linearly polarised such that it exits the polarising prism through one of its arms. This can be described by the following Jones Matrix calculation,

$$\overline{E}_{out} = \overline{R}(-\phi)\overline{M}_w\overline{R}(\phi)\overline{R}(-\theta)\overline{M}_\Gamma\overline{R}(\theta)\overline{E}_{in}, \tag{2.80}$$

where all the elements are the same as for balanced detection apart from M_w which now represents a half wave plate. A detector is then used to detect radiation that

exits the polarising cube through the fully extinguished output arm. When terahertz radiation is present the phase rotation induced within the ZnTe crystal causes some radiation to exit the polariser through the, previously extinguished, arm of the polarising cube. This radiation is then incident upon the detector. Using balanced detection the measurable signal could be defined as $S = \left|\overline{E}_{out,x}\right|^2 - \left|\overline{E}_{out,y}\right|^2$ whereas now the measurable signal is defined as simply $S = \left|\overline{E}_{out,x,y}\right|^2$. Using Eq. (2.76) it is possible to derive an expression for the terahertz field strength as a function of the measured signal,

$$S = \frac{1}{2} E_0 e^{-\frac{i3}{4}\pi}(-2i \sin \Gamma), \tag{2.81}$$

where E_0 is the intensity of the probe laser on the ZnTe surface. When combined with Eq. (2.75) this leaves

$$S = \frac{1}{2} E_0 e^{-\frac{i3}{4}\pi}\left(-2i \sin\left(\frac{\pi d}{\lambda_0} n_0^3 r_{41} E_T\right)\right). \tag{2.82}$$

Whilst this detection system is not as sensitive as balanced detection it does enable spatial mapping of the terahertz radiation to be performed. This spatial mapping can be achieved by using a two dimensional CCD camera which images the ZnTe crystal surface. The phase rotation imposed onto the optical probe beam only occurs when in spatial areas where the probe beam overlaps with terahertz radiation.

2.5 Photoconductive Antenna Generation

Photoconductive antennas (PCAs) are common sources of pulsed terahertz radiation. A PCA consists of a semiconducting material with a set of electrodes attached to the surface. This semiconducting material is held under a high electrical bias field via a voltage which is applied to the electrodes. The antenna is photoexcited by an ultrafast laser with photons that have a larger energy than the bandgap, thus liberating charge carriers from the valence band into the conduction band. Whilst in the conduction band the charge carriers are able to accelerate under the applied electrical bias field. Maxwell's equations state that an accelerating charge will emit radiation. This is the principle underlying mechanism that allows terahertz radiation to be generated from PCAs. The charge carriers continue to accelerate in the conduction band until they drop back down into the valence band. The time that the charge carriers remain in the conduction band is called the recombination lifetime and is wholly governed by the semiconductor material properties.

The two processes that govern the length of time that the charge carriers can accelerate for are interband scattering and screening. Interband scattering as the

name suggests describes the process through which charge carriers collide and scatter off other carriers and defects within the material. Having collisions within the conduction band reduces the mean free path of the electrons. This in turn can help to broaden the bandwidth of the generated terahertz pulse, as it effectively shortens generated radiations temporal profile. For the scattering process to be dominant or have a noticeable effect their must exist a very large electron density within the conduction band or a large number of defects within the material. Screening describes a process through which the electric field created by the non-uniform spatial density of charge carriers effects their acceleration due to the applied bias field. This can be seen in Fig. 2.12, where the red dots represent the holes and the blue dots represent electrons. As can be seen the electrons and holes are initally attracted towards the positivly and negativly charged electrodes respectivley. This causes a build up of electrons and holes around these electrodes in turn producing a large charge carrier density, and along with that a large electric field. This electric field causes the charge carriers to attempt to spread out, effectivly slowing or stopping their motion towards the electrode. This reduces the duration of the charge carriers acceleration and therefore increases the bandwidth of the generated terahertz radiation.

Generally, these recombination lifetimes are much larger than 100 fs and contribute towards the temporal structure of the generated terahertz pulse. Due to the recombination lifetime generally being much longer than that of the temporal duration of the excitation laser pulse, which is typically on the order of 30–100 fs, and temporal tuning imposed by the excitation laser is smeared out. This makes PCAs unsuitable for applications that require temporal tuning of the terahertz radiation imposed by the excitation laser radiation.

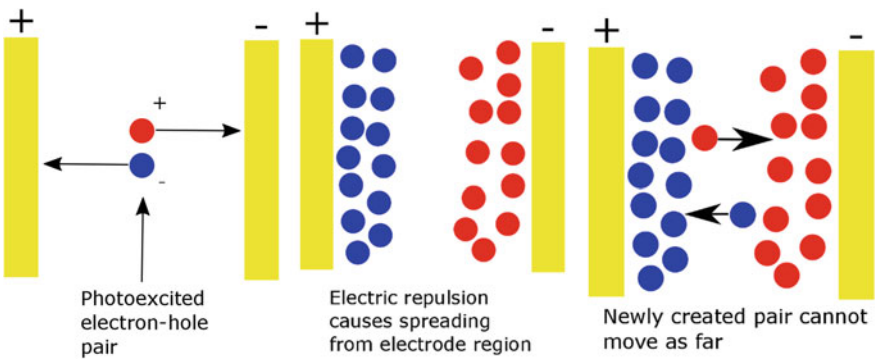

Fig. 2.12 Schematic diagram showing the effects of screening. Here the *blue circles* represent electrons whilst the *red circles* represent holes. As can be seen a build-up of negatively charged electrons exists around the +ve electrode whilst a build-up of positively charged holes exist around the −ve electrode

The electric field of the generated radiation can be expressed as [21]

$$\frac{\partial^2}{\partial y^2}E(\omega) + \frac{\omega}{c^2}\epsilon_0 E(\omega) = -i\omega\mu_0 J(\omega), \tag{2.83}$$

where $E(\omega)$ is the terahertz electric field, ω is the angular frequency and $J(\omega)$ is the current surge across the PCA. This expression is valid as long as the antenna has an aperture much larger than the wavelength of the generated terahertz radiation and the bias field across the antenna is uniform. A final condition that the terahertz field strength is much smaller than that of the applied bias field is also required as this description does not account for interactions between the liberated charges and generated terahertz radiation [21].

The current surge across the wafer as a function of time, $J(t)$, can be expressed by the non-equilibrium distribution of the free carriers within the antenna. This takes the form

$$J(t) = \frac{\hbar e}{4\pi^3}\int k_z\left[\frac{f_e}{m_e} - \frac{f_h}{m_h}\right]dk, \tag{2.84}$$

where e is the charge of an electron, k_z is the momentum vector of the charge carrier resolved into the z direction, f_e and f_h are the distribution of the free electrons and holes antenna respectively and m_e and m_h are the effective masses of the electrons and holes respectively. Making the assumption that $m_e \ll m_h$ enables the second term within the bracket to be ignored leaving,

$$J(t) = \frac{\hbar e}{4\pi^3}\int \frac{k_z f_e}{m_e}dk. \tag{2.85}$$

In order to further calculate the form of $J(t)$ the form of f_e must be approximated. This can be done by assuming a Boltzmann distribution of carriers, which takes the form,

$$\frac{\partial}{\partial t}f_e + \left(\frac{\hbar k}{m_e}\frac{\partial}{\partial r} + \frac{e}{\hbar}\frac{\partial}{\partial k}\right)f_e = -\Gamma(f_e - f_{eo}) + \Phi \mathrm{f}_e + G(t)\frac{\pi^2\delta(k-k_0)}{k_0^2}, \tag{2.86}$$

where Γ is the recombination rate, Φ is the inverse lifetime and $G(t)$ is the generation rate. The generation rate describes the flux of photons that have an energy larger than the semiconductor band gap and are incident upon the surface of the antenna. By considering the quantities that describe the laser pulse such as the intensity, I_0, the group velocity, v_0, and temporal duration, Δ, as well as the quantities that govern semiconductor-laser interaction such as absorption, α, and reflectivity, R, the generation rate can be expressed as [21],

$$G(t) = \frac{\alpha(1-R)I_0}{\hbar\omega_0} e^{\alpha y} e^{-\frac{t}{2\Delta^2}}. \tag{2.87}$$

Now by using Eq. (2.85) it is possible to express $J(t)$ in the frequency,

$$J(\omega) = \frac{e}{m_e} E_0[\Phi(k_0 - i\omega)]^{-1}[\Gamma(k_0) + \Phi(k_0) - i\omega]^{-1} G(\omega). \tag{2.88}$$

The Fourier transform of Eq. (2.87) can be taken yielding an expression which describes the generation rate in the frequency domain:

$$G(\omega) = \frac{\alpha(1-R)I_0}{\hbar\omega_0} e^{-\alpha y} e^{\frac{\omega^2\Delta^2}{2}} e^{\frac{i\omega}{2\Delta^2}}. \tag{2.89}$$

The above expression can now be used to form an expression for the terahertz electric field generated by the PCA in the frequency domain,

$$\begin{aligned} E(\omega) = &-\sqrt{\frac{\mu_0}{\epsilon_0}} A(\omega) \left[1 - \frac{i\omega(n+n_0)}{\alpha c}\right]^{-1} \\ &\times \frac{2n\left[1 - \frac{i\omega(n_0+n_e)}{\alpha e}\right]}{n+n_e^2} e^{\frac{i\omega n d}{c}} \left[1 - r^2 e^{\frac{i2\pi d\omega}{c}}\right]^{-1}, \end{aligned} \tag{2.90}$$

where $n_0 = \frac{c}{v_0}$, $n = \sqrt{\epsilon}$ and $n_e = \sqrt{\epsilon_0}$ and represent the refractive indices inside and outside the wafer respectively and $r = n - n_e/n + n_e$. The variable $A(\omega)$ contains the excitation radiation parameters and can be expressed as follows,

$$A(\omega) = \frac{\frac{e^2}{m_e} E_0(1-R)I_0\Delta}{\hbar\omega_0} \tau\tau_p e^{-\frac{\omega^2\Delta^2}{2}} (1 - i\omega\tau)^{-1} \left(1 - i\omega\tau_p\right)^{-1}, \tag{2.91}$$

where τ and τ_p represent the inverse lifetime, Φ and the inverse relaxation lifetime, Γ, respectively [21].

2.6 Longitudinally Polarised Radiation

Typically the electric fields of a propagating electromagnetic field in free space, light, are thought of as only having transversely polarised components. This means that the electric field lines point orthogonally to the direction of the propagation of the electromagnetic field. This, however, is not completely correct as all forms of free space propagating electromagnetic radiation, apart from azimuthally polarised radiation, have electric fields with longitudinally polarised components, i.e. electric

field components that are orientated in the direction of the propagating electromagnetic field. This can be seen by analysing

$$\nabla \cdot \overline{E}(x, y, z) = \rho_f, \tag{2.92}$$

where $\overline{E}(x, y, z)$ is an electric field in Cartesian spatial co-ordinates (x, y, z) and ρ_f is the density of free charges in the space occupied by the field. As this is a field propagating in free space, ρ_f can be set to zero. Therefore Eq. (2.13) states that the total spatial gradient of the electric field is zero, this means that the field lines cannot begin or end leaving two possible options. The first is that the field carries on to an infinite spatial extent and the second is that the field lines loop round and in doing so create a component of the field that points in the direction of propagation.

To investigate the form of the longitudinally polarised electric field component Eq. (2.92) can be rearranged by splitting $\overline{E}(x, y, z)$ and ∇ into their orthogonally polarised components i, j and k such that,

$$\frac{\partial}{\partial x}\hat{i}E(x, y, z) + \frac{\partial}{\partial y}\hat{j}\overline{E}(x, y, z) + \frac{\partial}{\partial z}\hat{k}E(x, y, z) = 0. \tag{2.93}$$

where i, j and k lie along the x, y and z axes respectively. Rearranging for the longitudinal component, k, subsequently yields,

$$E_k(x, y, z) = -\int_{-\infty}^{\infty} \nabla_{\perp} E_{\perp}(x, y, z)dz + C(x, y), \tag{2.94}$$

where $\perp$ denotes the linear combination of i and j and $C(x, y)$ is an unknown constant due to the integration. This constant however does not vary in z and so for pulsed radiation it can be said to be zero. This is because for pulsed radiation $E_k(x, y, z)$ and $E_{\perp}(x, y, z)$ must be zero at some z and for this to be true $C(x,y)$ must also be zero at that z and because it does not vary in z must therefore be zero for all z.

As can be seen from Eq. (2.94) the longitudinally polarised electric field component depends strongly upon the spatial gradient of the transversely polarised electric field component and in fact is maximised when the spatial gradient of the transversely polarised electric field component is maximised. This attribute is in fact apparent in electromagnetic modes with strong transverse gradients. Modes such as the radially polarised Laguerre-Gaussian 01 (LG01*) mode contain strong spatial gradients on axis and strong longitudinal fields have been observed on the axis of such modes [20]. Effects such as the tight focusing of radiation can also increase the amount of the electric field that can be resolved into the longitudinal direction. Again this has been observed in both complex modes with strong transverse gradients as well as simple standard Gaussian beams [22].

2.7 Acceleration of Charged Particles

A charged particle is a particle that is able to interact with an electromagnetic field. Within this section the acceleration of charged particles by external electromagnetic fields is discussed. For simplicity only electrons are considered, and assumed to be a point-like particle with no spatial dimension. To examine how an electron is influenced by an external electromagnetic field two properties of the electron must first be defined. Firstly its charge; the charge of the electron determines the strength of the interaction between an electromagnetic field and the electron. Secondly the electron mass is describes as resistance of the electron to a change in velocity.

In Newtonian physics the mass of a particle is constant and independent of velocity or acceleration. This is commonly referred to as the rest mass of the particle and for an electron denoted m_e. To describe the acceleration of an electron first one must be able to define its position in space. This is done in Cartesian co-ordinates and defined as a vector $\bar{x}$. Following this the velocity of the particle can be defined as $\bar{v}$ where

$$\bar{v} = \frac{\partial \bar{x}}{\partial t}. \tag{2.95}$$

Newton's first law of motion states that the velocity of a particle will remain constant unless an external force acts upon the particle. Momentum, $\overline{P}$, is now introduced as a quantity which describes how much force is needed to change the velocity of a particle and can be expressed as [23]

$$\overline{P} = m_e \bar{v}. \tag{2.96}$$

Newton's second law of motion now defines the force, $\overline{F}$, as [23]

$$\overline{F} = \frac{\partial \overline{P}}{\partial t}. \tag{2.97}$$

To understand how the force applied to a particle relates to a change in its velocity two quantities are introduced, the first being kinetic energy, $\overline{E}_k$, and the second being work done which is the change in kinetic energy, $\Delta\overline{E}_k$. The work done to a particle by a force can be described as [23]

$$\Delta\overline{E}_k = \int \overline{F} d\bar{x}. \tag{2.98}$$

By assuming that the mass of a particle is not a function of its velocity, which for now can be assumed, and by defining $\overline{E}_k = 0$ when $\bar{v} = 0$ the kinetic energy of a particle can be written as

$$\overline{E}_k = \frac{1}{2} m_e \overline{v}^2. \tag{2.99}$$

The act of placing a charged particle into a static electromagnetic field with potential energy $\overline{U}$ enables the exchange of energy between the particle and field. The sum of the kinetic energy and potential energy must always be constant and is defined as the total energy, $\overline{E}$. Noting that the field is static, i.e. $\frac{\partial \overline{U}}{\partial t} = 0$, it is possible to express the potential energy as a function of the work done,

$$\nabla \overline{E}_k = -\frac{\partial \overline{U}}{\partial \overline{x}}. \tag{2.100}$$

Here it is now possible to decompose the vectors onto the three Cartesian co-ordinate axes such that,

$$E_{k,x} = \frac{\partial}{\partial x} U_x, \tag{2.101}$$

$$E_{k,y} = \frac{\partial}{\partial y} U_y, \tag{2.102}$$

$$E_{k,z} = \frac{\partial}{\partial z} U_z. \tag{2.103}$$

Commonly it is attractive to accelerate a particle in one direction. It can be seen from the above equations that in order to do so the potential of the field must therefore be orientated in that direction. For instance taking z to be the desired direction of electron beam propagation it can be seen that the accelerating potential must also lie along the z axis.

2.7.1 Relativistic Motion

As described above charged particles can be described by three quantities, their position and velocity at a fixed time $(\overline{x}, \overline{v}, t)$. In Newtonian physics the amount of energy needed to accelerate a particle from $E_{k,z}(t = 1)$ to $E_{k,z}(t = 2)$ is not dependent upon the initial kinetic energy. This, whilst being a good approximation at low energies, does not hold for high energies when the velocity of the particle becomes a noticeable proportion of the speed of light. In such cases the mass of a particle is no longer independent of the velocity, but in fact can be expressed as a function of it,

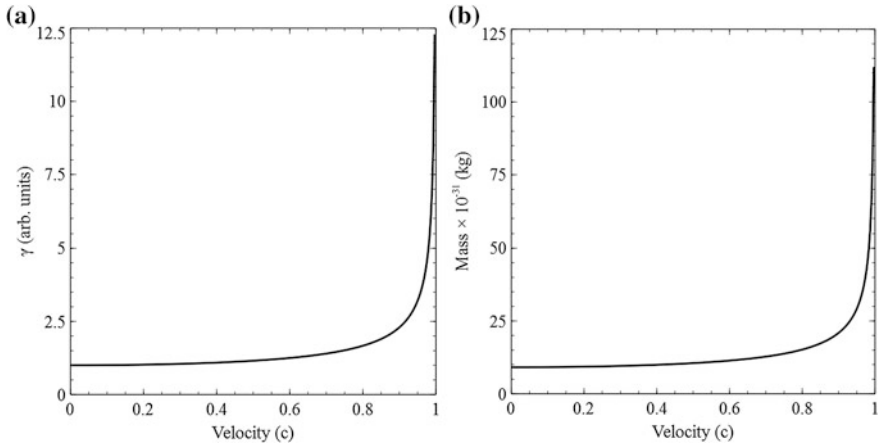

Fig. 2.13 Simulations produced to show **a** γ as a function of velocity and **b** the mass of an electron as a function of velocity

$$m = \gamma m_e, \tag{2.104}$$

where γ is a dimensionless quantity which describes the velocity of a particle as a fraction of the speed of light and can be expressed as

$$\gamma = \frac{1}{\sqrt{(1-\beta^2)}}, \tag{2.105}$$

where

$$\beta = \frac{v}{c}. \tag{2.106}$$

The relationship between γ and v can be seen in Fig. 2.13a. As can be seen in Fig. 2.13b for low velocities, velocities less than approximately half the speed of light, the mass of an electron remains constant and does not change appreciably as a function of velocity. However when the velocity of the electron approaches c its mass rapidly starts to increase tending towards infinity.

Whilst this does not change the relationship between force and momentum it does change the definition of momentum such that now,

$$\overline{P} = \gamma m_e \overline{v}. \tag{2.107}$$

Noticing now that as the velocity of the electron approaches c its momentum increases with respect to the velocity of the electron. Therefore the energy of the particle must be defined as

$$E = \gamma m_e c^2. \tag{2.108}$$

The kinetic energy is now the total energy minus the rest energy, $m_e c^2$, of the electron,

$$E_k = m_e c^2(\gamma - 1). \tag{2.109}$$

2.7.2 Acceleration Within an Electromagnetic Field

To analyse how an electron is accelerated by an electromagnetic field the change in momentum is calculated instead of the velocity. This is because in the relativistic regime there is very little change in the velocity of an electron where as there is a large change in the energy of an electron. The change in momentum over time is expressed as

$$\frac{\partial \overline{P}}{\partial t} = -q_e(\overline{E} + \overline{v} \times \overline{B}), \tag{2.110}$$

where

$$\overline{P} = \gamma mc\beta. \tag{2.111}$$

The change in γ which relates to the velocity of the particle is given as

$$\frac{\partial \gamma}{\partial t} = -\frac{q_e}{m_e c^2}\overline{v} \cdot \overline{E}, \tag{2.112}$$

As previously described an electron will be accelerated in the direction of the electric field. Therefore for co-linear acceleration with a propagating field the electric field radiation should have a strong on-axis component. Such components are present in modes such as radially polarised modes and Hermite-Gaussian TEM_{01} (HG01) modes. The electric field from a HG01 mode can be expressed in terms of its transverse, r, and longitudinal, z, field components as

$$E_r = \frac{4E_0\omega_0 r}{\sqrt{2\omega^2(z)}} e^{\left(-\frac{r^2}{\omega^2(z)}\right)} \sin(\phi), \tag{2.113}$$

$$E_z = \frac{4E_0\omega_o}{\sqrt{2}k\omega^2(z)} e^{\left(-\frac{r^2}{\omega^2(z)}\right)} \left[\left(1 - \frac{2r^2}{\omega^2(z)}\right)\cos\phi - \frac{2zr^2}{Z_R\omega^2(z)}\sin\phi\right]. \tag{2.114}$$

If we assume that the electrons being accelerated are on axis, i.e. are positioned at $r = 0$, then $E_r = 0$ and the accelerating field becomes,

$$E_z = \frac{4E_0\omega_o}{\sqrt{2}k\omega^2(z)}\cos\phi. \tag{2.115}$$

This can now be used in conjunction with Eq. (2.110) such that it becomes

$$\frac{\partial \overline{P}_z}{\partial t} = -q_e\left(\frac{4E_0\omega_o}{\sqrt{2}k\omega^2(z)}\cos\phi + \overline{v}\times\overline{B}\right), \tag{2.116}$$

and as we are now only considering on-axis acceleration in the z direction the magnetic field becomes zero leaving,

$$\frac{\partial \overline{P}_z}{\partial t} = -q_e\left(\frac{4E_0\omega_o}{\sqrt{2}k\omega^2(z)}\cos\phi\right). \tag{2.117}$$

Equation (2.112) now also becomes

$$\frac{\partial \gamma_z}{\partial t} = -\frac{q_e}{m_e c^2}v_z \cdot \frac{4E_0\omega_o}{\sqrt{2}k\omega^2(z)} \tag{2.118}$$

These two equations describe the on-axis longitudinal acceleration of a relativistic electron by a radially polarised electric field. The change in the momentum of the electron as a function of time describes how much the particle is accelerated over a given time period whilst the change in γ_z describes change in the energy and velocity of the particle over a given time period. Whilst both these quantities are linked and can provide the same information they are commonly used in different ways to obtain different information about the acceleration of a particle.

2.7.3 *Acceleration with Terahertz Radiation*

Typically electron bunches have temporal profiles on the order of 0.5–10 ps and are accelerated using radio frequency electromagnetic radiation. Radio frequency electromagnetic radiation typically has temporal periods on the 10's ns scale. This mismatch in temporal periods makes it very difficult to perform fine temporal tuning of the longitudinal profile of the electron bunch. It would therefore be attractive to use radiation with a much shorter period to perform fine temporal tuning of the longitudinal profile, providing the ability to produce ultrashort electron bunches and electron bunches with unique longitudinal profiles. Such bunches would be very useful in fields such as pump-probe spectroscopy, synchronisation and particle therapy.

Whilst radiation with extremely small temporal periods, such as optical radiation, would be ideal for the fine temporal tuning of relativistic electron bunches the fact that the period is much less than the longitudinal profile of the electron bunch causes a new problem. This problem involves the phase slippage of the particle bunch relative to the modulation radiation; as they co-propagate the electron bunch travels slightly slower than the modulating radiation. This causes the electron bunch to slip through many cycles of the modulating radiation meaning it experiences, on average, as many positive field areas as it does negative field areas essentially providing zero net modulation.

Electromagnetic radiation with periods similar to that of the electron bunch, 0.5–10 ps, such as terahertz radiation does not present either of these problems. The temporal profile of terahertz radiation is short enough that fine temporal adjustments to the longitudinal profile of the electron bunch can be carried out. In fact depending on the generation source these temporal manipulations can be directly imposed by a pump optical laser and if a laser driven terahertz source is chosen this inherently enables sub 10 fs electron beam—laser beam synchronisation. However its temporal period is not so short as to enable electron bunches to co-propagate and experience a number of positive and negative cycles. Electron bunches with typical energies of approximately 25 MeV are able to co-propagate with a terahertz pulse centred around 0.3 THz for approximately 1 m before they fall half a cycle out of phase [24]. This length only increases as the electron bunch energy increases and for the same energy is much higher than the 30 μm coherence length which would be achievable with 800 nm optical radiation.

Whilst terahertz radiation appears to be an obvious answer to being able to provide fine scale longitudinal energy modulation to relativistic electron bunches, only in the last few years have terahertz sources capable of producing useable field strengths being developed. Sources able to produce terahertz field electric strengths in excess of 500 $kVcm^{-1}$ are required for noticeable and useful energy modulation of relativistic bunches. These sources must also have a unique and complex polarisation state allowing them to have an on-axis strong longitudinally polarised electric field component. As of now such a source has not been developed; however the individual components required have. It would therefore be important to further investigate the development of such a source which is the main aim of this work.

References

1. D.J. Griffiths, *Introduction to electrodynamics* (Prentice Hall, New Jersey, 1999)
2. R.W. Boyd, *Nonlinear Optics* (Academic Press, 2003)
3. J.D. Jackson, *Classical Electrodynamics*, 3rd edn. (John Wiley & Sons, 1999)
4. S. Casalbuoni, H. Schlarb, B. Schmidt, P. Schmuser, B. Steffen and A. Winter, Numerical studies on the electro-optic detection of femtosecond electron bunches. Phys. Rev. Spec. Top. Accelerators Beams **11**, 072802 (2008)
5. J. Hebling, G. Almäsi, I.Z. Kozma, Velocity matching by pulse front tilting for large-area THz-pulse generation. Opt. Express **10**, 1161 (2002)

6. H. Hirori, A. Doi, F. Blanchard, K. Tanaka, Single-cycle terahertz pulses with amplitudes exceeding 1 MV/cm generated by optical rectification in $LiNbO_3$. Appl. Phys. Lett. **98**, 091106 (2011)
7. J. Oden, J. Meilhan, J. Lalanne-Dera, J. Roux, F. Garet, J. Coutaz, F. Simoens, Imaging of broadband terahertz beams using an array of antenna-coupled microbolometers operating at room termperature. Opt. Express **21**, 4817 (2013)
8. S. Cherednichenko, A. Hammar, S. Bevilacqua, A room temperature bolometer for terahertz coherent and incoherent detection. IEEE Trans. Terahertz Sci. Technol. **1**, 395 (2011)
9. F. Simoens, *THz Bolometer Detectors* (Springer, 2013)
10. L. Fernandes, P. Kaufmann, R. Marcon, A.S. Kadaka, A. Marun, R. Godoy, E.C. Bortolucci, M.B. Zakia and J. A. Diniz, Photometry of THz radiation using Golay cell detector, in *General Assembly and Scientific Symposium, 2011 XXXth URSI*, Istanbul, 2011
11. W.J. Stillman, M.S. Shur, Closing the gap: plasma wave electronic terahertz detectors. J. Nanoelectron. Optoelectron. **2**, 209 (2007)
12. C. Winnewisser, P. Uhd Jepsen, M. Schall, V. Schyja, H. Helm, Electro-optic detection of THz radiation in LiTaO3, LiNbO3 and ZnTe. Appl. Phys. Lett. **70**, 3069 (1997)
13. G. Gallot, J. Zhang, R.W. McGowan, T.- I. Jeon, D. Grischkowsky, Measurements of the THz absorption and dispersion of ZnTe and their relevance to the electro-optic detection of THz radiation. Appl. Phys. Lett. **74**, 3450 (1999)
14. A. Leitensotorfer, S. Hunsche, J. Shah, M.C. Nuss, W.H. Knox, Detectors and sources for ultrabroadband electro-optic sampling: experiment and theory. Appl. Phys. Lett. **74**, 1516 (1999)
15. S. Park, M.R. Mellock, A.M. Weiner, Comparison of terahertz waveforms measured by electro-optic and photoconductive sampling. Appl. Phys. Lett. **73**, 3184 (1998)
16. N. Yasumatsu, S. Watanabe, Precise real-time polarization measurement of terahertz electromagnetic waves by a spinning electro-optic sensor. Rev. Sci. Instr. **83**, 023104 (2012)
17. S. Casalbuoni, H. Schlarb, B. Schmidt, P. Schmuster, B. Steffen and A. Winter, *Numerical studies on the electro-optic sampling of relativistic electron bunches* (DESY, TELSA Report, 2005)
18. D.A. Walsh, M.J. Cliffe, E.W. Snedden, D.M. Graham, W.A. Gillespie and S.P. Jamison, Role of misalignment-induced angular chirrp in the electro-optic detection of THz waves. Opt. Express **22**, 12028 (2014)
19. Z. Gui-hua and W. Ya-min, Study of jones matrix of the birefringent crystal, in *Symposium on Photonics and Optoelectronics, 2009. SOPO 2009*. (Wuhan, 2009)
20. M.J. Cliffe, A. Rodak, D.M. Graham and S. P. Jamison, Generation of longitudinally polarized terahertz radiation with field amplitudes exceeding 2 kV/cm. Appl. Phys. Lett. **105**, 1191112 (2014)
21. V.N. Trukhin, A.V. Andrianov and N. N. Zinov'ev, Generation of terahertz radiation by a photoconductive antenna. Acta. Phys. Pol. A **113**, 921 (2008)
22. S. Winnerl, R. Hubrich, M. Mittendorff, H. Schneider and M. Helm, Universal phase relation between longitudinal and transverse fields observed in focused terahertz beams. New J. Phys. **14**, 103049 (2012)
23. J.R. Taylor, *Classical Mechanics*. (University Science Books, 2004)
24. S.P. Jamison, M.J. Cliffe, D.M. Graham, T. Thakker, B. Muratori, Y.M. Saveliev , R.J. Smith, W.R. Flavell, D.J. Holder, D. Newton and A. Wolski, Phase space manipulation with laser-generated terahertz pulses, in *34th International Free Electron Laser Conference*, Japan (2012)

http://www.springer.com/978-3-319-48642-0

Longitudinally Polarised Terahertz Radiation for Relativistic Particle Acceleration

Cliffe, M.J.

2017, XIII, 150 p. 86 illus., 67 illus. in color., Hardcover
ISBN: 978-3-319-48642-0